Supporting Information for "Managing financial risk tradeoffs for hydropower generation using snowpack-based index contracts"

Andrew L. Hamilton[1,2], Gregory W. Characklis[1,2], and Patrick M. Reed[3]

[1]Department of Environmental Sciences and Engineering, University of North Carolina at Chapel Hill, Chapel Hill, North Carolina, USA

[2]Center on Financial Risk in Environmental Systems, University of North Carolina at Chapel Hill, Chapel Hill, North Carolina, USA

[3]Department of Civil and Environmental Engineering, Cornell University, Ithaca, New York, USA

Contents of this file

1. Text S1 to S5
2. Tables S1 to S4
3. Figures S1 to S9

Corresponding author: Andrew L. Hamilton, andrew.hamilton@unc.edu

Introduction

This text provides additional methodological details related to synthetic snow water equivalent depth (SWE) observations (Section S1), synthetic hydropower production (Section S2), synthetic wholesale power prices (Section S3), the financial simulation model used to translate hydropower generation and power prices into net revenues (Section S4), and the method used to price index contracts (Section S5). Tables S1-S4 provide parameter estimates for the models described in Sections S1-S3. Figures S1-S3 provide support for Sections S1, S2, and S5 respectively, while Figures S4-S9 provide additional results beyond the main text.

S1: Synthetic snow water equivalent depth (SWE)

Both February 1 and April 1 snow water equivalent depth (SWE) measurements were available for each year 1952-2016, except 1963, a total of 64 years. The historical SWE record is not found to exhibit any statistically significant trend in at an annual time step ($p = 0.45$ and 0.59 for February 1 and April 1, respectively), nor does it exhibit significant autocorrelation at an annual time step ($p > 0.05$ on Ljung-Box test for all lags up to 15 years for both February 1 and April 1 observations). Let $\mathbf{s_F}$ and $\mathbf{s_A}$ be the $n = 64$ years of February 1 and April 1 snow water equivalent depth (SWE) observations described by the stationary random variables S_F and S_A. These two variables are inherently correlated through the seasonal snow accumulation process. It is important that any synthetic SWE observations capture the dependency structure of the original dataset.

Copulas provide a convenient way to capture this dependency. Let

$$H(S_F, S_A) = C[F_F(S_F), F_A(S_A)] \tag{1}$$

where H is the joint cumulative distribution function (cdf) of S_F and S_A, F_F and F_A are their marginal cdf's, and C is the copula which dictates the dependency between the variables. Sklar showed that any joint distribution can be written in this form (Sklar, 1973), which allows us to separate the treatment of the marginal distributions from their dependency structure.

The marginal distributions are found to be well described by gamma distributions, with probability density function (pdf)

$$f(S) = \frac{S^{k-1}e^{-x/\theta}}{\theta^k \Gamma(k)} \tag{2}$$

where $\Gamma()$ is the gamma function and k and θ are the shape and scale parameters, respectively. The parameter estimates $\hat{k}$ and $\hat{\theta}$ are calculated independently for February and April using maximum likelihood estimation, and can be found in Table S1. We fail to reject the null hypothesis that the historical observations are drawn from the fitted gamma distribution using the Kolmogorov-Smirnov test of goodness of fit, for both February 1 ($p = 0.54$) and April 1 ($p = 0.98$) SWE.

Next, the copula describing the dependency structure between the two variables is estimated. Copula estimation consists of two steps: selection of a functional form and estimation of the functional parameters. A wide variety of functional forms have been studied in the literature (Frees & Valdez, 1998; Genest & Favre, 2007). We choose to use the Gaussian copula, part of the larger metaelliptical class of copulas, for a variety of reasons. Firstly, it is flexible and easily extensible to more than two variables, unlike other classes such as Archimedean copulas. Although the current work only uses two variables (S_F and S_A), we would like our workflow to be easily extensible to larger datasets in the future. Secondly, it is simple and allows for efficient generation of synthetic data. Lastly, it is shown to effectively capture the empirical dependency between February 1 and April 1 SWE, as will be shown shortly.

In Equation 1, H is a cumulative distribution function (cdf), taking on values from 0 to 1, as are the arguments to the copula ($F_F(S_F)$ and $F_A(S_A)$). Thus, the copula maps $(0,1)^2 \rightarrow (0,1)$. Rewriting the copula arguments as U_F and $U_A \in (0,1)$, we can define the Gaussian copula

$$C(U_F, U_A) = \Phi_{2,\rho}(\Phi_1^{-1}(U_F), \Phi_1^{-1}(U_A)) \tag{3}$$

where Φ_1^{-1} is the inverse of the standard univariate normal cdf Φ_1, and $\Phi_{2,\rho}$ is the bivariate joint cdf of standard normal variables with correlation ρ.

This shows that the copula only depends on the cumulative probabilities U, independently of the marginal distributions F. This allows for efficient sampling through the following algorithm (Wang, 1999): (1) Sample values (z_F, z_A) from the bivariate standard normal distribution with correlation ρ. For more than two variables, use the correlation matrix Σ. (2) Calculate cumulative probabilities $(u_F = \Phi_1(z_F), u_A = \Phi_1(z_A))$. (3) Calculate the SWE values with equivalent cumulative probabilities under the gamma marginal distributions, $(s_F = F_F^{-1}(u_F), s_A = F_A^{-1}(u_A))$. This algorithm can be scaled up efficiently to generate many synthetic observations using modern statistical software.

The correlation is the only parameter that needs to be estimated for a Gaussian copula. Following Genest et al., (Genest, Favre, Béliveau, & Jacques, 2007), we estimate the correlation using Kendall's tau, a non-parametric analogue of correlation,

$$\hat{\tau}_{FA} = \frac{C_{FA} - D_{FA}}{C_{FA} + D_{FA}} \tag{4}$$

where C_{FA} and D_{FA} are the number of concordant and discordant pairs, respectively, in the historical dataset. The pair (i, j) are defined as concordant if $(S_{F,i} - S_{F,j})(S_{A,i} - S_{A,j}) > 0$, and discordant otherwise. The estimate $\hat{\tau}$ is an asymptotically normal and unbiased estimator for the population value τ. Now the correlation estimate $\hat{\rho}$ can be calculated using the relation:

$$\hat{\rho} = \sin\left(\frac{\pi\hat{\tau}}{2}\right) \tag{5}$$

The appropriateness of the Gaussian copula can be judged using a graphical approach proposed by Genest & Favre (Genest & Favre, 2007). The approach is similar to the popular QQ-plot. Define the normalized order statistics,

$$W_i = \frac{1}{n}\#\{j : S_{F,j} <= S_{F,i}, S_{A,j} <= S_{A,i}\} \tag{6}$$

In other words, W_i gives the fraction of observations with SWE values that are less than or equal to observation i in both February and April. W_i takes values on $(0, 1]$, and defines the empirical copula. The first step in the graphical approach is to calculate $\mathbf{W}_{data}$, the $n = 64$ dimensional vector of normalized order statistics for the historical data. Then $M = 10,000$ synthetic samples of n years are generated from the fitted copula, and the order statistics $(\mathbf{W}_{fitted,1}, ..., \mathbf{W}_{fitted,M})$ are calculated. Each $\mathbf{W}$ vector is sorted from smallest to largest. The mean, 5th percentile, and 95th percentile are calculated for each of the $n = 64$ positions, yielding the vectors $\mathbf{W}_{fitted,mean}$, $\mathbf{W}_{fitted,p5}$, and $\mathbf{W}_{fitted,p95}$. Now the QQ-plot can be generated by scattering $\mathbf{W}_{data}$ against $\mathbf{W}_{fitted,mean}$. If the observed data's dependency structure is well described by the fitted copula, then the plotted points should fall close to the one-to-one line. Sampling error bounds are estimated by $\mathbf{W}_{fitted,p5}$, and $\mathbf{W}_{fitted,p95}$. Figure S1 suggests that the fitted copula is a good fit for the historical SWE observations.

S2: Synthetic hydropower generation

In order to capture the relationship between snowpack and monthly hydropower generation, separate predictors are developed for each month of the water year, using the 29 water years available, 1988-2016.

For the first and last month of the water year (October and September), no statistically significant relationship (at a 10% significance level) is found between February 1 or April 1 SWE and hydropower generation. For these months expected generation is constant and the model can be written

$$G_{m,y}^{constant} = \beta_{0,m} + r_{m,y} \tag{7}$$

where $G_{m,y}^{constant}$ is the hydropower generation in month m of water year y, $\beta_{0,m}$, is the constant expected generation, and $r_{m,y}$ is the residual. The parameter estimate $\hat{\beta}_{0,m}$ is the sample mean.

The second class of model is a linear relationship between SWE and hydropower generation, written

$$G_{m,y}^{linear} = \beta_{0,m} + \beta_{1,m} S_{A/F,y} + r_{m,y} \tag{8}$$

where $S_{F/A,y}$ is either the February 1 or April 1 SWE value for water year y, and $\beta_{0,m}$ and $\beta_{1,m}$ are the intercept and slope parameters, respectively, to be estimated via linear regression. In cases where both February 1 and April 1 models are statistically significant (at a 10% significance level), the best model is selected by minimizing the Akaike information criterion (AIC). We find that February 1 SWE is the best linear predictor for November, December, and January, while April 1 SWE is used for February, July, and August.

For the peak snowmelt months of March through June, a clear upper threshold behavior is evident in the scatter plot of SWE vs hydropower generation. This reflects that fact that in the wettest years, some water may need to be spilled without generating hydropower. For this reason, generation is fit to April 1 SWE by minimizing the sum of squared residuals for the following piecewise linear model:

$$G_{m,y}^{piecewise} = \begin{cases} \beta_{0,m} + \beta_{1,m} S_{A,y} + r_{m,y} & , S_{A,y} < (\beta_{2,m} - \beta_{0,m})/\beta_{1,m} \\ \beta_{2,m} + r_{m,y} & , else \end{cases} \tag{9}$$

where $\beta_{0,m}$ and $\beta_{1,m}$ are the intercept and slope parameters of the increasing segment and $\beta_{2,m}$ is the expected generation in the constant segment above the SWE threshold.

The threshold is calculated based on these parameters as $(\beta_{2,m} - \beta_{0,m})/\beta_{1,m}$. Parameter estimates for each monthly model described above can be found in Table S2, and models are visualized in Figure S2.

As described in the main text, the model residuals for the historical observations are deseasonalized based on month and SWE. The deseasonalized residuals are then fit to an autoregressive (AR) model in order to remove autocorrelation. Because all data points have been deseasonalized, the process has zero mean and thus no constant term. Only one and three month lags are found to be statistically significant (at the 5% level), resulting in the following linear regression:

$$\tilde{r}_t = \varphi_1 \tilde{r}_{t-1} + \varphi_3 \tilde{r}_{t-3} + \varepsilon_t \tag{10}$$

where $\tilde{r}_t$ is the deseasonalized residual for month t in the historical record, $\tilde{r}_{t-1}$ and $\tilde{r}_{t-3}$ are the deseasonalized residuals 1 and 3 months prior to observation t, and φ_1, and φ_3 are the regression parameters. The final model residuals ε_t are not found to exhibit significant autocorrelation (Ljung-Box test, $p > 0.18$ for all lags up to 36 months) and are not found to differ significantly from normality (Shapiro-Wilk test, $p = 0.79$). Parameter estimates for the AR model can be found in Table S3.

S3: Synthetic wholesale power prices

The seven years of historical power prices are first log-transformed and deseasonalized, as described in the main text. Let x_t be the deseasonalized log-prices ($\tilde{p}_{m,y}$ in the main text) for the month t in the time series corresponding to (m, y). Now the deseasonalized log prices can be fit to a seasonal autoregressive moving average (SARMA) model. Let SARMA$(p, q)(P, Q)_{12}$ represent a SARMA model that combines an autoregressive model with lags of $(1, .., p)$ months and $12{*}(1, .., P)$ months, and a moving average error model with lags of $(1, .., q)$ and $12{*}(1, .., Q)$ months. Because all data points have been deseasonalized, the process has zero mean and thus no constant term. This model can be written:

$$x_t = \sum_{i=1}^{p} \varphi_i x_{t-i} + \sum_{j=1}^{P} \varphi_{12j} x_{t-12j} + \sum_{k=1}^{q} \theta_k \varepsilon_{t-k} + \sum_{l=1}^{Q} \theta_{12l} \varepsilon_{t-12l} + \varepsilon_t \tag{11}$$

where φ_L is the autoregressive parameter for lag L, θ_L is the moving average error parameter for lag L, and ε_t is the prediction error for month t. In order to choose the appropriate model order, regression parameters are estimated for all combinations of (p, q, P, Q), where each parameter is either 0 or 1 (a total of 16 models). From among the four models with similarly low Bayesian Information Criterion (BIC) values ($BIC_{(1,1,0,1)} = 123.35$, $BIC_{(1,1,1,0)} = 123.90$, $BIC_{(1,0,0,1)} = 125.15$, $BIC_{(1,0,1,0)} = 125.71$), the SARMA$(1,0),(0,1)_{12}$ model is selected as the model which best matches the monthly patterns of the historical data. This model consists of a single lag of one month for the autoregressive model, plus a moving average error model with a single lag of twelve months, and can be written:

$$x_t = \varphi_1 x_{t-1} + \theta_{12}\varepsilon_{t-12} + \varepsilon_t \tag{12}$$

Parameter estimates for the SARMA model can be found in Table S4. The residuals from the SARMA model are not found to exhibit significant autocorrelation ($p > 0.1$ on Ljung-Box test for all lags up to 36 months) and are not found to deviate significantly from a normal distribution (Shapiro-Wilk test, $p = 0.51$).

S4: Revenue model

Given synthetic hydropower generation G_t and wholesale power prices P_t, the simulated revenues R_t can be written:

$$R_t = r^M D^M + r^I D_t^I + P_t(G_t - D^M - D_t^I) \tag{13}$$

where r^M and r^I are the fixed volumetric rates for municipal customers and irrigation districts, respectively, and D^M and D_t^I are the fixed municipal demand and variable irrigation district demand.

The municipal rate (r^M = \$0.1049/kWh) and demand (D^M = 998.405 GWh/year) and are taken as their 2016 values from public financial statements (San Francisco Public Utilities Commission, 2016). The demand is calculated as the sum of four classes: "General Fund Rate Subsidized," "Enterprise Rate," "Non-city Agencies," and "Moccasin/City of Riverbank," and the fixed rate is calculated as a sales-weighted average of the four class rates. Given that heating and cooling tend to drive variability in electricity demand, retail demand is fairly constant throughout the year due to the mild Bay Area climate in which temperatures do not deviate widely on a seasonal basis (San Francisco Public Utilities Commission, 2015). In light of this, it is assumed for this work that the demand is spread evenly across the year.

The fixed rate for Modesto and Turlock Irrigation Districts (MTID) is taken as the sales-weighted average value of the 2016 rates for the two districts in the financial statement (San Francisco Public Utilities Commission, 2016). In this work, we assume that MTID purchases a fixed fraction of excess hydropower generation above municipal demand, so that demand is fit to the model:

$$D_t^I = c \max(G_t - D^M, 0)\delta_{P_t > r_I} \tag{14}$$

where c, the fraction of excess hydropower generation that MTID will purchase, is a parameter to be fit using linear regression. $\delta_{P_t > r_I}$ is an indicator function ensuring that MTID only purchases power from the utility when the fixed rate is lower than the wholesale power rate. Using the historical annual sales volumes from 2010-2016 (San Francisco Public Utilities Commission, 2016), we find $c = 0.483$ ($p < 0.01$). This means that 48.3% of the excess power in any given month is sold to MTID. The other 51.7% of excess power is sold into the wholesale market.

S5: Index contract pricing

In order to find the contract loading and the corresponding reference value for the SWE index, which separates positive payouts at low SWE values and negative payouts at high SWE values, the capped contract for differences (CFD) structure is decomposed into two parts. The CFD can be seen as the sum of a "long put" position and a "short capped call" position, as shown in Supporting Information Figure S3. The long put position provides linearly increasing payouts when the SWE index falls below a threshold called the "strike", in exchange for an annual premium, while the short call position requires making payments when the SWE index falls below the strike, in return for receiving an annual premium. A cap on call payments is applied at some higher threshold. The payouts shown in Figure S3 have been netted of premiums. The strike for both contracts is set at the 50th percentile of the SWE distribution (24.53 inches), while the cap is set at the 95th percentile (48.44 inches). The swap contract is created by summing these two positions.

In order to price the premiums, the Wang transform, as described in Section 2.6.3 of the main text, can be performed numerically for any payout cumulative distribution function (cdf) $F(x)$. In this case, $F(x)$ is the empirical cdf built from the synthetic contract payout time series, which is itself a function of the synthetic SWE index time series. For example, for the put contract,

$$x = V * \max(k - s, 0) \tag{15}$$

where V is the contract slope in dollars per inch, k is the strike value set as the median of the SWE distribution, and s is the SWE value observed. The contract premium is then calculated as the expected value of x under the risk-adjusted probability density function (pdf) $f^*(x)$. Thus, the expected net payout, x minus the premium, is equal to zero under the risk-adjusted pdf. After calculating the premiums for the long put and short capped call, the CFD structure is equivalent to the sum of these two positions. The "loading" in Section 2.6.3 of the main text is equal to the premium for the long put position minus the premium for the short capped call position. The reference value of SWE for the CFD is the intersection of net payout function with the x-axis.

Following other work on weather derivative contracts (Baum, Characklis, & Serre, 2018; Foster, Kern, & Characklis, 2015; Wang, 2002), the market price of risk parameter is set as $\lambda = 0.25$ for the baseline value for the put contract in this study. However, values between $\lambda = 0$ (no loading) and 0.5 (high loading) are included in the sensitivity analysis, as described in Section 2.9 of the main text, and the effect of this parameter on the contract structure can be seen in Figure 5 of the main text. Because the short capped call position is used in payment for the long put position, rather than a separate hedging contract, it is priced in the actuarially fair manner (i.e., $\lambda = 0$). If a risk loading were applied to this position, this would imply that the contract seller is willing to accept a lower (expected value) premium if it comes in variable payments rather than fixed payments, which is unlikely in practice.

References

Baum, R., Characklis, G. W., & Serre, M. L. (2018). Effects of Geographic Diversification on Risk Pooling to Mitigate Drought-Related Financial Losses for Water Utilities. *Water Resources Research*, *54*, 1–19. doi: 10.1002/2017WR021468

Foster, B. T., Kern, J. D., & Characklis, G. W. (2015). Mitigating hydrologic financial risk in hydropower generation using index-based financial instruments. *Water Resources and Economics*, *10*, 45–67. doi: 10.1016/j.wre.2015.04.001

Frees, E. W., & Valdez, E. A. (1998). Understanding relationships using copulas. *North American Actuarial Journal*, *2*(1), 1–25. doi: 10.1080/10920277

.1998.10595667

Genest, C., & Favre, A.-C. (2007). Everything You Always Wanted to Know about Copula Modeling but Were Afraid to Ask. *Journal of Hydrologic Engineering*, *12*(4), 347–368. doi: 10.1061/(asce)1084-0699(2007)12:4(347)

Genest, C., Favre, A. C., Béliveau, J., & Jacques, C. (2007). Metaelliptical copulas and their use in frequency analysis of multivariate hydrological data. *Water Resources Research*, *43*(9), 1–12. doi: 10.1029/2006WR005275

San Francisco Public Utilities Commission. (2015). *Hetch Hetchy Water & Power, Financial Statements, June 30, 2015 and 2014* (Tech. Rep.).

San Francisco Public Utilities Commission. (2016). *Comprehensive Annual Financial Report, Fiscal Years Ended June 30, 2016 and 2015* (Tech. Rep.).

Sklar, A. (1973). Random Variables, Joint Distribution Functions, and Copulas. *Kybernetika*, *9*(6), 449–460.

Wang, S. S. (1999). "Understanding Relationships Using Copulas," Edward Frees and Emiliano Valdez, January 1998. *North American Actuarial Journal*, *3*(1), 137–142. doi: 10.1080/10920277.1999.10595785

Wang, S. S. (2002). A Universal Framework for Pricing Financial and Insurance Risks. *ASTIN BULLETIN*, *32*(2), 213–234. doi: 10.2143/AST.32.2.1027

Tables

Table S1. Parameter estimates for synthetic snow water equivalent (SWE) model. All parameters unitless.

Parameter	Date	Symbol	Estimate
Gamma shape	February 1	$\hat{k}_F$	2.9167
	April 1	$\hat{k}_A$	5.1693
Gamma scale	February 1	$\hat{\theta}_F$	6.4355
	April 1	$\hat{\theta}_A$	5.7539
Copula correlation	NA	$\hat{\rho}_{FA}$	0.8017

Table S2. Parameter estimates for monthly models of synthetic hydropower generation based on SWE. Units for $\hat{\beta}_{0,m}$ and $\hat{\beta}_{2,m}$ are GWh per month, and units for $\hat{\beta}_{1,m}$ are GWh per month per inch of SWE.

Month	SWE predictor	Model	$\hat{\beta}_{0,m}$	$\hat{\beta}_{1,m}$	$\hat{\beta}_{2,m}$
October	NA	Constant	83.76	NA	NA
November	Feb. 1	Linear	59.29	0.9182	NA
December	Feb. 1	Linear	36.97	3.251	NA
January	Feb. 1	Linear	43.05	3.639	NA
February	Apr. 1	Linear	14.57	3.942	NA
March	Apr. 1	Piecewise	48.67	4.691	230.8
April	Apr. 1	Piecewise	91.66	3.774	226.4
May	Apr. 1	Piecewise	126.8	3.179	235.9
June	Apr. 1	Piecewise	33.29	6.045	232.8
July	Apr. 1	Linear	45.54	3.532	NA
August	Apr. 1	Linear	89.94	0.8156	NA
September	NA	Constant	93.68	NA	NA

Table S3. Parameter estimates for autoregressive model for synthetic hydropower generation residuals. All parameters unitless.

Parameter	Symbol	Estimate
Lag-1 weight	$\hat{\varphi}_1$	0.5405
Lag-3 weight	$\hat{\varphi}_3$	-0.1203

Table S4. Parameter estimates for seasonal autoregressive moving average (SARMA) model for deseasonalized log power prices. All parameters unitless.

Parameter	Symbol	Estimate
Lag-1 autoregression weight	$\hat{\varphi}_1$	0.8663
Lag-12 moving average error weight	$\hat{\theta}_{12}$	-0.3740

Figures

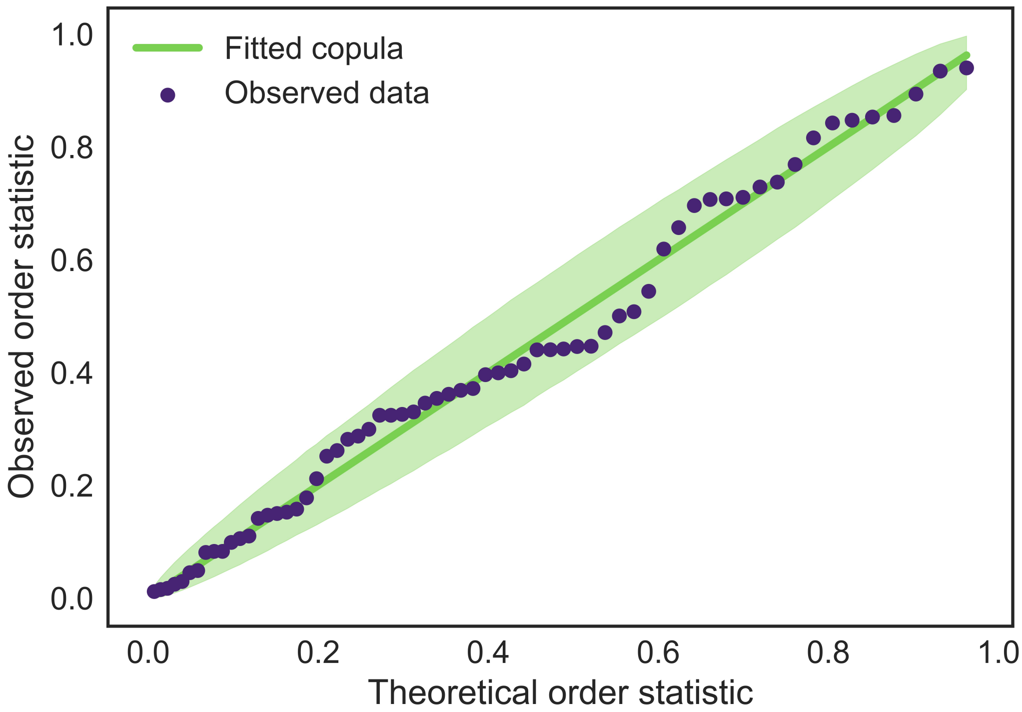

Figure S1. QQ-plot showing fit between normalized order statistics of the observed data and the fitted Gaussian copula. Shaded region shows the 5th and 95th percentile sampling error for the Gaussian copula.

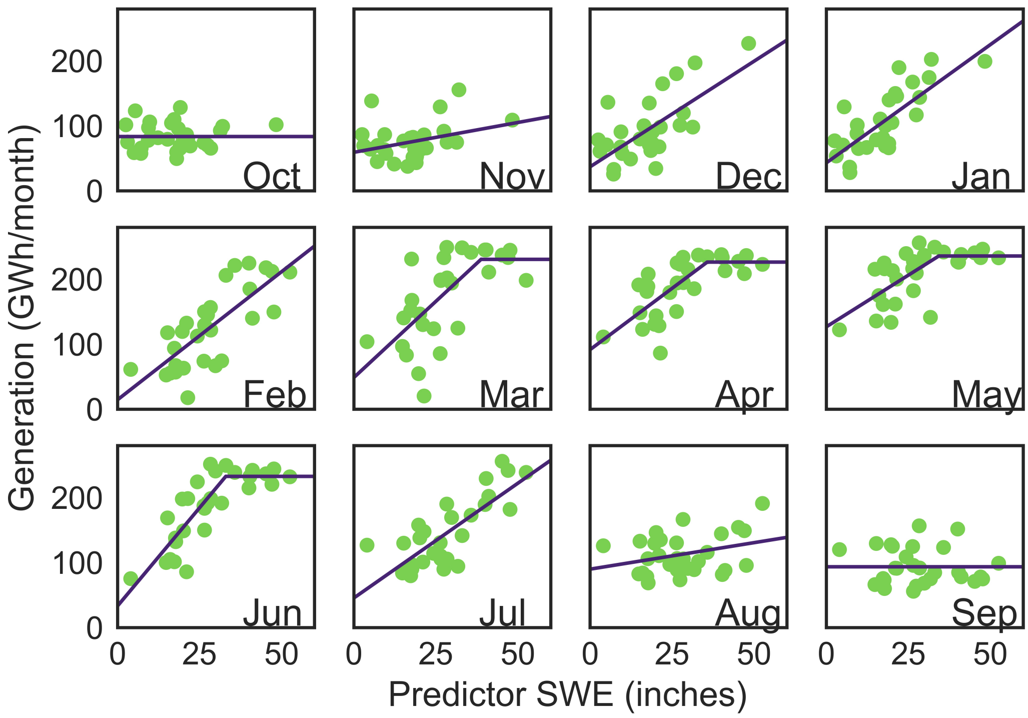

Figure S2. Hydropower generation as a function of snow water equivalent depth (SWE) for each month in the water year. Fitted models (purple lines) shown against historical data (green dots). The x-axis "predictor SWE" is February 1 SWE for October through January, and April 1 SWE for February through September.

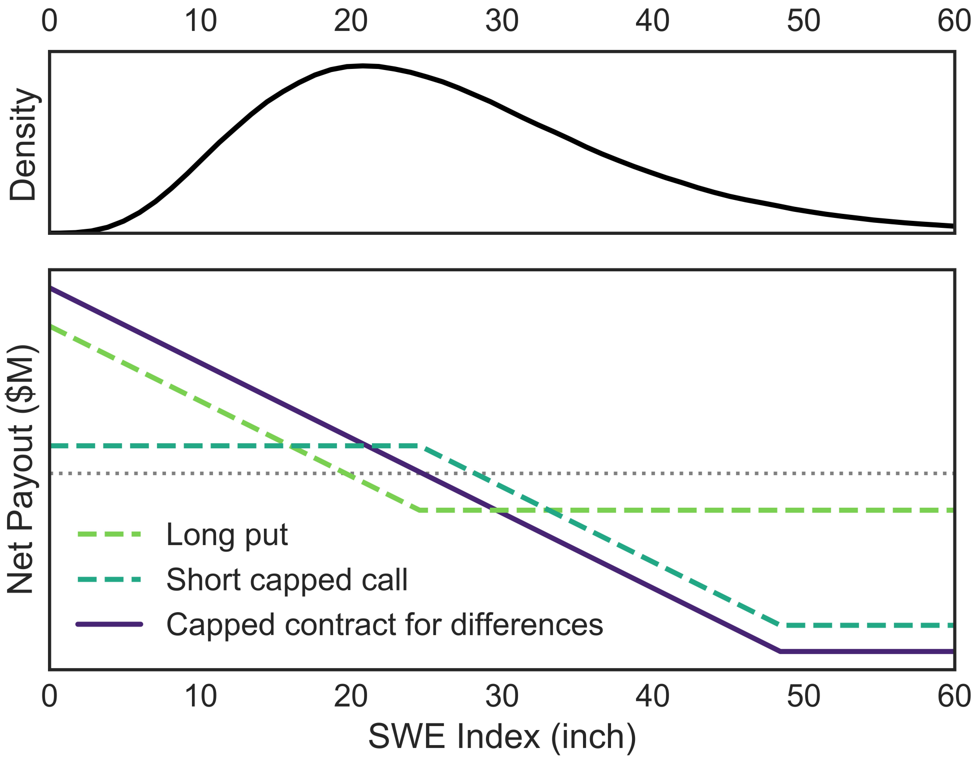

Figure S3. (top) Probability density for SWE index, a weighted average of February 1 and April 1 observations. (bottom) Net payouts for three possible contract structures: a long put position with a strike at the 50th percentile (24.53 inch), a short call position with a strike at the 50th percentile and a cap at the 95th percentile (48.44 inch), and a capped contract for differences (CFD) equal to the sum of the two previous positions.

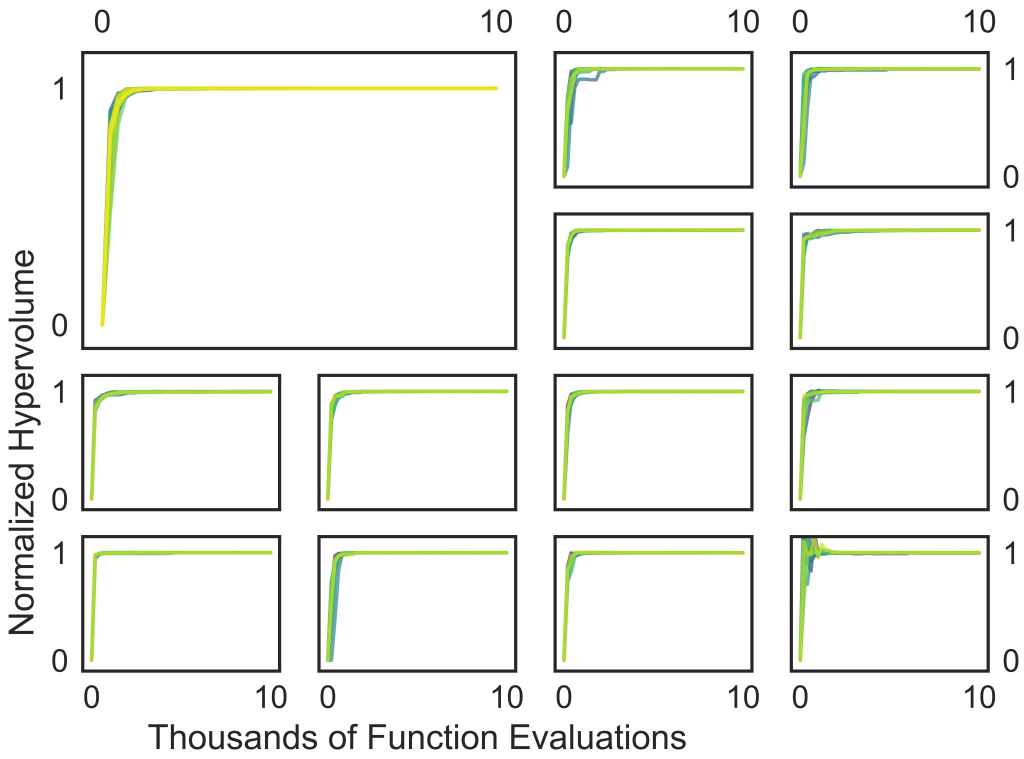

Figure S4. (top left) Normalized hypervolume of approximate Pareto sets from Borg MOEA with 50 random seeds for baseline state of world (SOW). (all others) Normalized hypervolume of approximate Pareto sets from Borg MOEA with 10 random seeds each for 12 randomly selected SOWs.

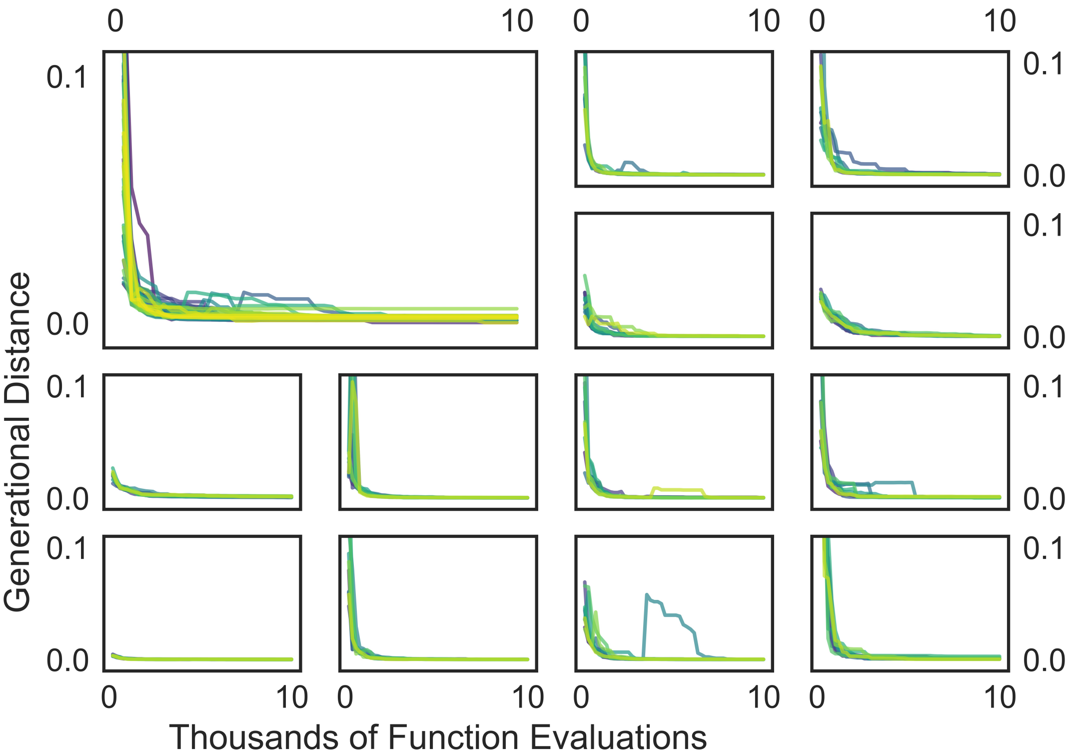

Figure S5. (top left) Generational distance metric for approximate Pareto sets from Borg MOEA with 50 random seeds for baseline state of the world (SOW). (all others) Generational distance metric for approximate Pareto sets from Borg MOEA with 10 random seeds each for 12 randomly selected SOWs.

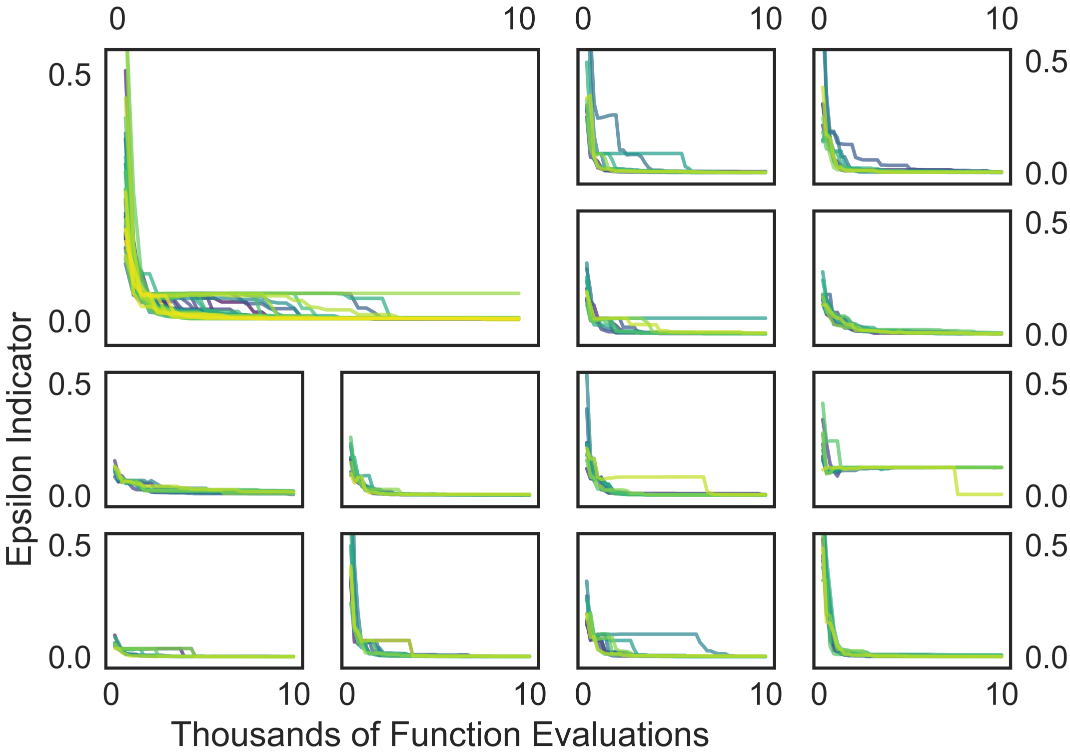

Figure S6. (top left) Epsilon indicator metric for approximate Pareto sets from Borg MOEA with 50 random seeds for baseline state of the world. (all others) Epsilon indicator metric for approximate Pareto sets from Borg MOEA with 10 random seeds each for 12 randomly selected SOWs.

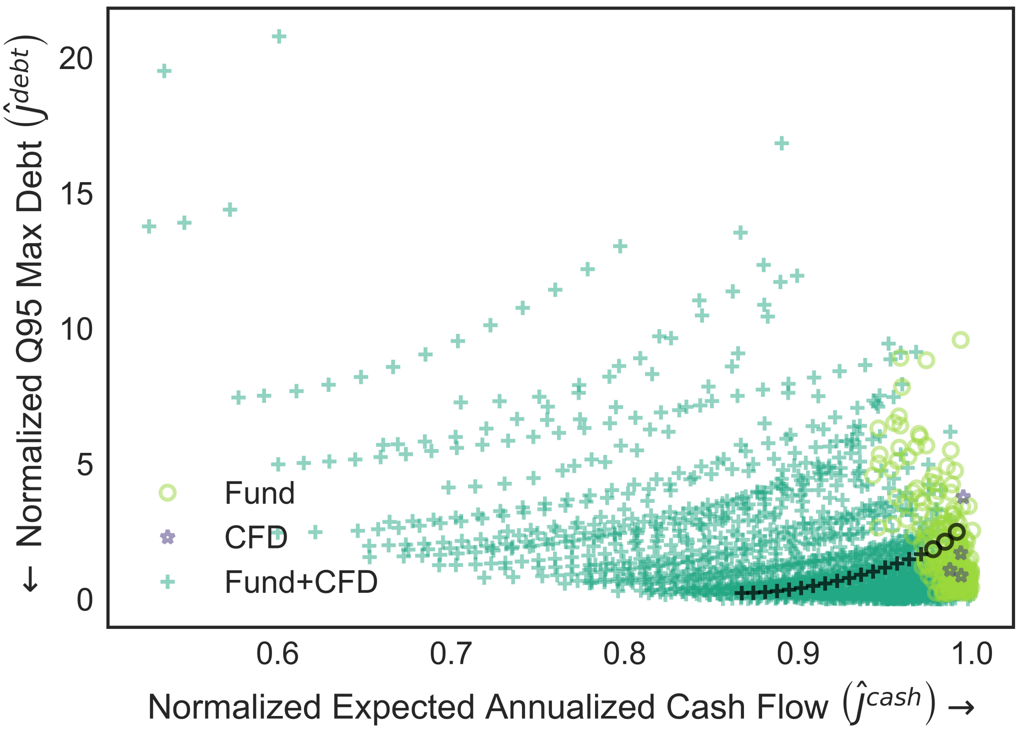

Figure S7. Same as Figure 10 from main text, but showing all unfiltered results.

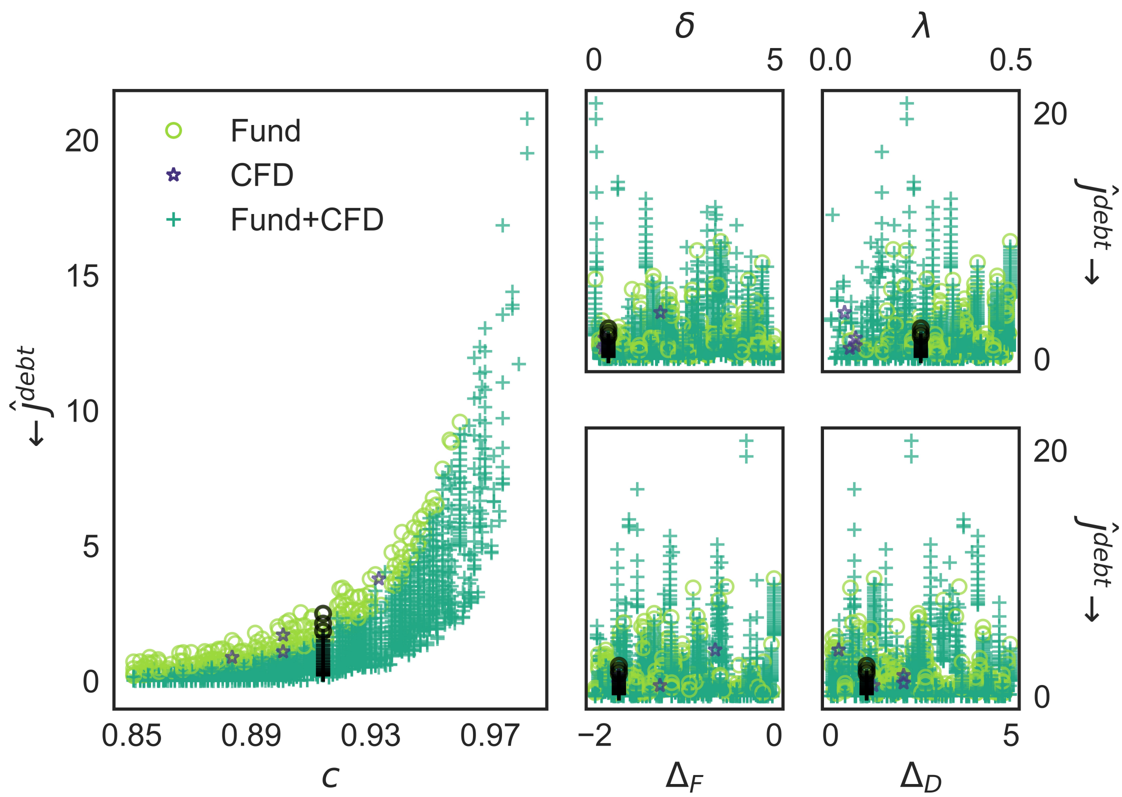

Figure S8. Same as Figure 11 from main text, but showing all unfiltered results.

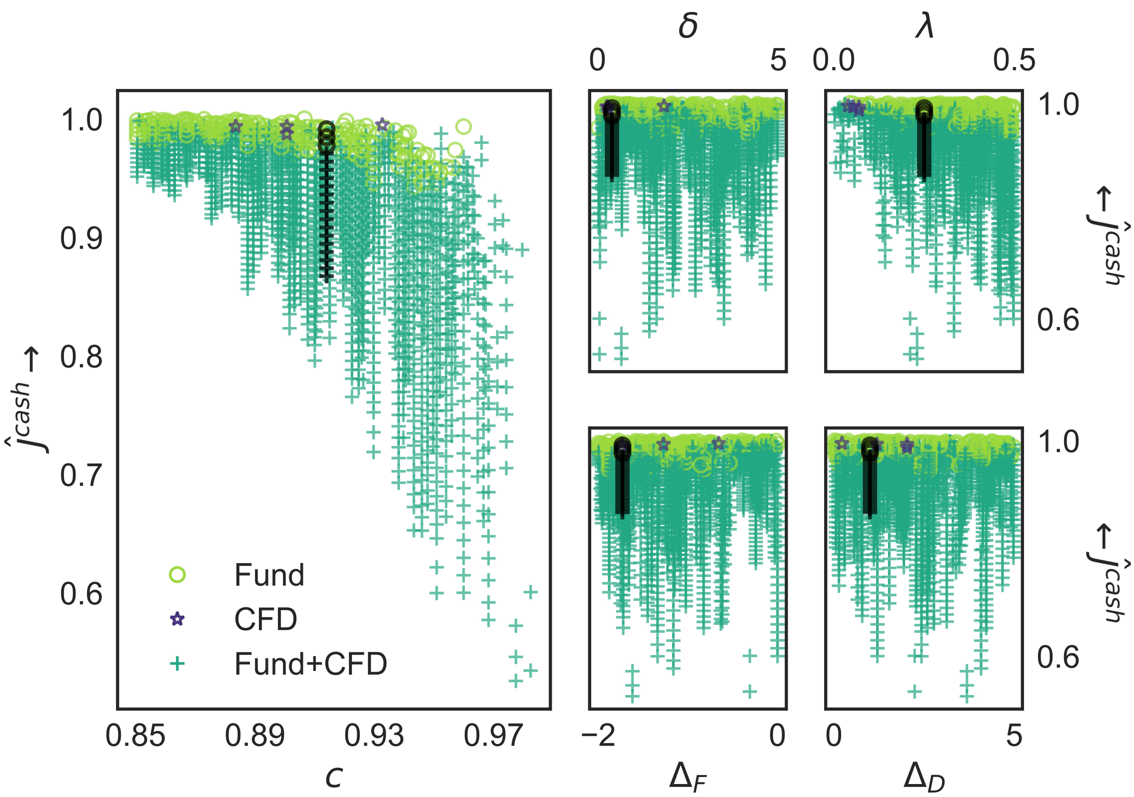

Figure S9. Same as Figure 12 from main text, but showing all unfiltered results.